Technical Report - Additional Mathematical Description for Paper "Wheel-Centric Protection: A Paradigm Shift in Vehicle Safety with Low-Level Wheel Trajectory Control"

Denis Efremov, Martin Klaučo, and Tomáš Haniš [*†]

1 Introduction

This document offers additional mathematical derivations for the baseline controller used in the "Experiments" section of the paper titled "Wheel-Centric Protection: A Paradigm Shift in Vehicle Safety with Low-Level Wheel Trajectory Control," submitted to IEEE TRANSACTIONS ON INTELLIGENT TRANSPORTATION SYSTEMS. It also discusses the lack of necessity for imposing spatial constraints on the rear axle.

The referenced paper focuses on formulating an environmental envelope and model predictive control frameworks for vehicle and wheel safety. The simulation experiments provided demonstrate that the resulting control strategy can be used for road or lane keeping and obstacle avoidance. However, the strategy is primarily designed for drivable obstacle avoidance, which refers to obstacles that can be driven over by the car body but not by the wheels, such as potholes.

2 Baseline Controller Description

The baseline controller is very similar to the one used in the referenced paper, but it has two key differences:

- The drivable road is defined using only the centerline and two distances: the maximum possible left and right deviations from this centerline. This concept is inspired by (but not fully copied) the idea of the environmental envelope described in [1]. In our paper, we define the left and right road boundaries independently, which allows for more flexible road configurations.
- All obstacles on the road are treated as undrivable, meaning that the vehicle will avoid each obstacle with its entire body, even in cases where only a pothole needs to be avoided. This is a traditional obstacle avoidance strategy, which is enhanced in our submitted paper.

2.1 Reference Model

The reference model is defined using a linear single-track framework with linearized coordinates and heading calculations. The model is represented as follows:

$$\dot{x}(t) = Ax(t) + Bu(t) + q, \tag{1}$$

*D. Efremov and T. Haniš, are with the Department of Control Engineering, Faculty of Electrical Engineering, Czech Technical University in Prague, 120 00 Nové Město, Czech Republic (e-mail: {denis.efremov, martin.klauco, tomas.hanis}@fel.cvut.cz

†M. Klaučo is with the Institute of Information Engineering, Automation, and Mathematics, Slovak University of Technology in Bratislava, Radlinskeho 9 82137 Bratislava, Slovakia (e-mail: martin.klauco@stuba.sk)

where the state and input vectors are combined as

$$x = \begin{bmatrix} \beta & r & p_{\mathrm{x}} & p_{\mathrm{y}} & \psi \end{bmatrix}^{\top}, \quad u = \delta, \tag{2}$$

and the system matrices are given by

$$A = \begin{bmatrix} -\dfrac{c_{\mathrm{f}}F_{\mathrm{zf}} + c_{\mathrm{r}}F_{\mathrm{zr}}}{mv} & \dfrac{l_{\mathrm{r}}c_{\mathrm{r}}F_{\mathrm{zr}} - l_{\mathrm{f}}c_{\mathrm{f}}F_{\mathrm{zf}}}{mv^2} - 1 & 0 & 0 & 0 \\ \dfrac{l_{\mathrm{r}}c_{\mathrm{r}}F_{\mathrm{zr}} - l_{\mathrm{f}}c_{\mathrm{f}}F_{\mathrm{zf}}}{I} & -\dfrac{l_{\mathrm{r}}^2c_{\mathrm{r}}F_{\mathrm{zr}} + l_{\mathrm{f}}^2c_{\mathrm{f}}F_{\mathrm{zf}}}{vI} & 0 & 0 & 0 \\ 0 & 0 & 0 & 0 & 0 \\ v & 0 & 0 & 0 & v \\ 0 & 1 & 0 & 0 & 0 \end{bmatrix}, \tag{3}$$

$$B = \begin{bmatrix} \dfrac{c_{\mathrm{f}}F_{\mathrm{zf}}}{mv} & \dfrac{l_{\mathrm{f}}c_{\mathrm{f}}F_{\mathrm{zf}}}{I} & 0 & 0 & 0 \end{bmatrix}^{\top}, \quad q = \begin{bmatrix} 0 & 0 & v & 0 & 0 \end{bmatrix}^{\top}. \tag{4}$$

Figures 1 and 2 illustrate the linearized single-track model and the notation for position and orientation states, with the associated variables and parameters detailed in Table 1.

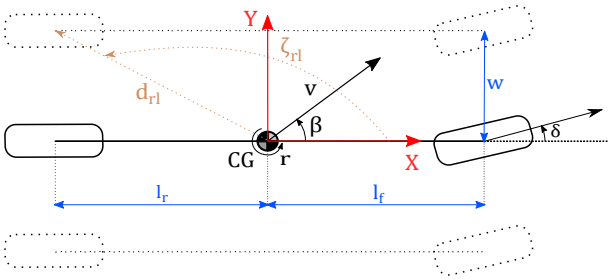

Figure 1: The single-track model (CG - the center of gravity).

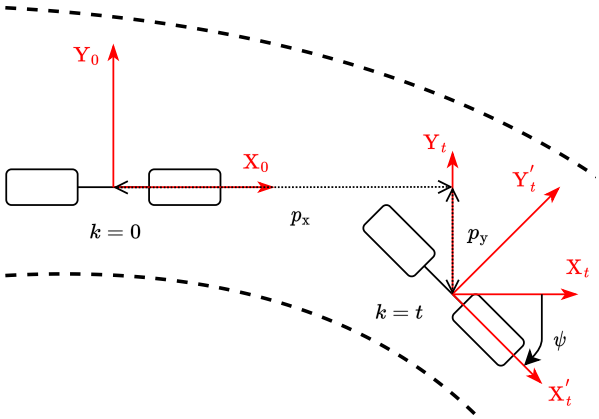

Figure 2: The inertial reference frame is set at the vehicle's initial position ($k = 0$). The car's position (p_{x} and p_{y}) and heading (ψ) are measured relative to this initial point.

Lateral forces on the wheels are approximated using nominal cornering stiffness coefficients $c_{\mathrm{f/r}}$ and load forces $F_{\mathrm{zf/zr}}$, both time-varying.

The MPC strategy is based on discrete-time vehicle dynamics defined as

$$x_{k+1} = A_{\mathrm{d}}x_k + B_{\mathrm{d}}u_k + q_{\mathrm{d}}, \tag{5}$$

which is obtained via Euler discretization of the continuous-time system (1).

Variable	Symbol	Units
Vehicle speed at CG	v	$\mathrm{m\,s^{-1}}$
Sideslip angle at CG	β	rad
Yaw rate at CG	r	$\mathrm{rad\,s^{-1}}$
Steering angle of the front axle	δ	rad
Load force of a wheel	F_z	N
Position coordinate w.r.t. inertial frame	p	m
Heading of the vehicle w.r.t. initial heading	ψ	rad
Distance from CG to a wheel	d	m
Angle from X-axis to a wheel	ζ	rad
Used subscriptions	**Subindex**	
Lateral or longitudinal direction	y or x	
Front or rear axle	f or r	
Left or right side	l or r	

Parameter	Symbol	Value	Units
Vehicle mass	m	1463	kg
Yaw moment of inertia	I	1968	$\mathrm{kg\,m^2}$
Distance from CG to [front/rear] axle	$l_{[\mathrm{f/r}]}$	0.97/1.57	m
[Front/rear] tire lateral nominal stiffness	$c_{\alpha[\mathrm{f/r}]}$	15.4/17.6	$\mathrm{rad^{-1}}$
Half of axle width	w	0.789	m

Table 1: Used notation and test vehicle parameters

2.2 MPC Formulation

The optimal control problem (OCP) for the baseline controller is formulated as follows:

$$\min_{u_0,\ldots,u_{N-1}} \sum_{k=0}^{N-1} \Big(R_1 \left|\delta_\mathrm{cmd} - u_k\right| + R_2(\delta_\mathrm{cmd} - u_k)^2 \tag{6a}$$

$$+ R_\mathrm{du}(u_k - u_{k-1})^2 + R_u u_k^2 + x_k^\intercal R_x x_k \Big) \tag{6b}$$

$$+ \sum_{k=0}^{N} \left[s_{\mathrm{i},k}^\intercal Q_\mathrm{i} s_{\mathrm{i},k} + s_{\mathrm{eo},k}^\intercal W Q_\mathrm{eo} s_{\mathrm{eo},k} + s_{\mathrm{eb},k}^\intercal Q_\mathrm{eb} s_{\mathrm{eb},k} \right] \tag{6c}$$

$$\text{s.t.} \quad x_{k+1} = A_\mathrm{d} x_k + B_\mathrm{d} u_k + q_\mathrm{d}, \tag{6d}$$

$$|u_k - u_{k-1}| \leq \Delta u_\mathrm{max} + s_\mathrm{i}, \tag{6e}$$

$$|u_k| \leq u_\mathrm{max}, \tag{6f}$$

$$s_{\mathrm{i},k} \geq 0, \tag{6g}$$

$$p'_{\mathrm{x},k} = p_{\mathrm{x},k} + l_\mathrm{f}, \tag{6h}$$

$$p'_{\mathrm{y},k} = p_{\mathrm{y},k}, \tag{6i}$$

$$(p'_{\mathrm{x},k} - p_{\mathrm{x}_{\eta_0}})^2 + (p'_{\mathrm{y},k} - p_{\mathrm{y}_{\eta_0}})^2 \geq W^{(\eta,\eta)}(r_\eta + w - s^{(\eta)}_{\mathrm{eo},k})^2, \tag{6j}$$

$$s_{\mathrm{eo},k} \geq 0, \tag{6k}$$

$$p'_{\mathrm{y},k} - a_3 p'^{(3)}_{\mathrm{x},k} - a_2 p'^{(2)}_{\mathrm{x},k} - a_1 p'_{\mathrm{x},k} \leq a_0 - \sigma + d_\mathrm{l} - w + s_{\mathrm{eb},k}, \tag{6l}$$

$$p'_{\mathrm{y},k} - a_3 p'^{(3)}_{\mathrm{x},k} - a_2 p'^{(2)}_{\mathrm{x},k} - a_1 p'_{\mathrm{x},k} \geq a_0 + \sigma - d_\mathrm{r} + w - s_{\mathrm{eb},k}, \tag{6m}$$

$$s_{\mathrm{eb},k} \geq 0, \tag{6n}$$

$$x_0 = \begin{bmatrix} \beta(t) & r(t) & 0 & 0 & 0 \end{bmatrix}, \tag{6o}$$

$$u_{-1} = u(t - T_\mathrm{s}) \tag{6p}$$

is defined over the prediction horizon N, where k denotes the prediction step and t represents the initial time.

The main goal of the controller (6) is to accurately track the commanded steering angle. The objective function (6a) achieves this by combining first and second norms relative to the reference signal δ_{cmd}.

Weights $R_{\mathrm{d}u}$ in (6b) penalize rapid changes in control inputs, promoting smoother driving, while R_u limits the use of extreme steering angles. Weight R_x minimizes sideslip angles to prevent excessive skidding.

To avoid infeasibility in the OCP, slack variables s_{i}, s_{eo}, and s_{eb} are introduced with high penalties Q_{i}, Q_{eo}, and Q_{eb}. The binary diagonal matrix W selectively activates obstacle constraints in the objective function, allowing prioritization of specific obstacles.

The basic controller formulation accounts for two obstacles ($\eta = 2$), adding constraints for each affected wheel and corresponding slack variables minimized in the objective function.

Constraints (6d) through (6i) apply for $k = 0, \ldots, N-1$, while constraints (6j) through (6n) are enforced for $k = 0, \ldots, N$. Constraint (6d) corresponds to the discretized linear single-track dynamics derived from (5). Inequalities (6e) and (6f) impose physical limits on control variables, ensuring protection against rapid changes (slew rate) and restricting values to their maximum allowable limits.

The key difference between the controller used in this work and the one in the submitted paper lies in constraints (6h) - (6n). The referenced paper focuses on avoiding obstacles individually with each wheel. In contrast, this implementation follows a more traditional approach, aiming to avoid obstacles with the entire vehicle. To achieve this, we define the midpoint of the front axle in constraints (6h) and (6i) and enforce obstacle avoidance for this point as described in (6j). Consequently, the obstacle size is significantly enlarged to account for the entire vehicle's dimensions.

Another modification in this work compared to the submitted paper is the implementation of road boundaries based on a central trajectory line, as presented in (6l) and (6m). The central line remains modeled as a cubic parabola, but the midpoint of the front axle is constrained to stay within the left and right boundaries. The left boundary is created by shifting the parabola horizontally using parameter d_{l}, and the right boundary is similarly defined using parameter d_{r}. The rest of the optimal control problem structure remains unchanged.

To ensure feasibility throughout the prediction horizon, constraints (6j) - (6n) are applied to the final state. The decision variable at the last step, u_N, is set equal to the input from the previous step, u_{N-1}, to compute x_{N+1} using (6d). The slack variables in (6g), (6k), and (6n) are defined as non-negative. The MPC problem is initialized with the initial condition in (6o), where $\beta(t)$ and $r(t)$ are the state measurements, and $u(t-T_{\mathrm{s}})$ is the control input from the previous sampling instant. All control strategy parameters are listed in Table 2.

3 Rear Wheels Constraints

In the referenced work and the baseline controller, constraints for the rear axle are not provided, primarily for three reasons.

Firstly, we decided to significantly reduce the number of inequality constraints and additional decision variables provided in the OCP for each pair of wheels and obstacles or wheels and road boundaries.

Secondly, the focus is on regular driving scenarios that do not involve high-performance lateral maneuvers like drifting, which typically occurs at higher sideslip angles (0.4 - 0.5 rad). When the sideslip angle surpasses certain stability thresholds, vehicle maneuvers become unsafe. These stability boundaries can be defined using concepts such as the handling envelope [2] or the driving envelope [3]. For the vehicle in our paper, the stability limit for the sideslip angle is around 0.2 - 0.3 rad. Beyond this point, the vehicle dynamics may become unsafe for less experienced drivers [3], potentially leading to drift and hazardous situations.

To account for potential discrepancies between the front and rear wheel tracks, among other factors, we introduced safe margins for both obstacles and road boundaries. Specifically, a margin of 0.2 m was used for obstacle avoidance, covering possible imprecisions, including differences between the front and

Parameter	Symbol	Value
Prediction horizon	N	20
Sampling time	T_s	0.05 s
Reference tracking linear weight	R_1	10^3
Reference tracking quadratic weight	R_2	10^3
Fast input change penalty	$R_{\mathrm{d}u}$	10^2
High input penalty	R_u	10^2
High state penalty	R_x	diag([50, 0, 0, 0, 0])
Slew slack penalization	Q_i	10^{10}
Envelope obstacle slack penalization	Q_eo	10^5
Envelope road boundary slack penalization	Q_eb	10^4
Slew rate limit for steering angle	Δu_max	$\frac{4\pi}{3} \cdot T_\mathrm{s}$ rad s^{-1}
Maximum steering angle	u_max	0.65 rad
Safe distance from road border	σ	0.2 m
Obstacle size (used constant for all the experiments)	$r_{1/2}$	2 m
Distance from the central trajectory line to the left/right road boundary	$d_{\mathrm{l/r}}$	1.75 m

Table 2: Control variables

rear wheel tracks. In the first experiment of the submitted paper, where the vehicle exhibits the highest sideslip angles, it is clear that on regular road segments, the sideslip angles are minimal, and the track distance remains within the safety margin (see Fig. 3). On the final segment, designed as a cornering section of a racing track, the driver applies brakes, and the maneuver requires high steering angles that result in higher sideslip angles. However, the difference between the tracks remains relatively small and within acceptable limits.

The third reason relates to the chosen reference model. To reduce the computational complexity of the resulting MPC, we opted for a linear single-track model, which accurately approximates vehicle movement at small sideslip angles. However, as sideslip angles increase, the model's accuracy diminishes. If constraints were applied to both axles (for each of the four wheels), the resulting control law would be overly conservative, limiting the use of larger steering angles.

For scenarios requiring higher precision in such difficult maneuvers (for example, for racing), a more accurate reference model should be employed. We recommend using a nonlinear single-track or even a twin-track model for such applications. However, it would increase the algorithm's demands from the computational point of view.

4 Acknowledgment

This work was supported in part by Toyota Motor Europe; in part by the Grant Agency of the Czech Technical University in Prague under Grant SGS22/166/OHK3/3T/13; in part by the Slovak Research and Development Agency under Grant APVV-21-0019; in part by the Scientific Grant Agency of the Slovak Republic under Grant VEGA 1/0239/24; and in part by the Ministry of Education, Youth and Sports of the Czech Republic, under Project 8X20037.

References

[1] S. M. Erlien, S. Fujita, and J. C. Gerdes, "Shared steering control using safe envelopes for obstacle avoidance and vehicle stability," *IEEE Transactions on Intelligent Transportation Systems*, vol. 17, no. 2, pp. 441–451, 2015.

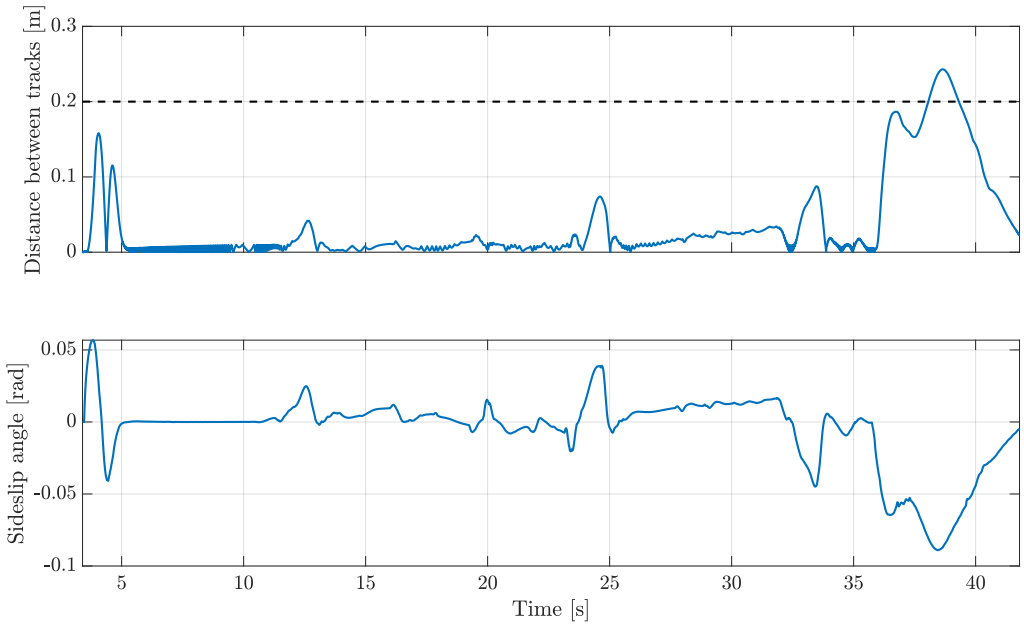

Figure 3: Sideslip angle of the vehicle and distance between tracks of the front left and rear left wheels during the first experiment from the submitted paper (Fig. 6 in the paper).

[2] C. E. Beal and J. C. Gerdes, "Model predictive control for vehicle stabilization at the limits of handling," *IEEE Transactions on Control Systems Technology*, vol. 21, no. 4, pp. 1258–1269, 2013.

[3] D. Efremov, T. Haniš, and M. Klaučo, "Vehicle and wheels stability defined using driving envelope protection algorithm," *IEEE Transactions on Intelligent Transportation Systems*, 2024.